Solid State Science and Technology, Vol. 22, No 1 & 2 (2014) 91-100
ISSN 0128-7389 | *http://journal.masshp.net*

STRUCTURAL, MAGNETIC AND ELECTRICAL PROPERTIES OF $PrMnO_3$/$Pr_{0.67}Ba_{0.33}MnO_3$ SINGLE AND BI-LAYER THIN FILMS

J. K. Wong, K. P. Lim, S. A. Halim, S. K. Chen, S. W. Ng,
H. M. Albert Gan and H. W. Chin.

Department of Physics, Faculty of Science, Universiti Putra Malaysia, 43400 UPM Serdang, Selangor, Malaysia

.

Corresponding author: wjenkuen@hotmail.com

ABSTRACT

The single and bi-layer manganite thin film of $PrMnO_3$ (PMO) and $Pr_{0.67}Ba_{0.33}MnO_3$ (PBMO) were fabricated on single crystal MgO oriented (100) substrate via pulsed laser deposition technique. In this work, the importance of stacking sequence in bi-layer manganite films of PMO and PBMO was reported. The unit cell of PMO experienced negative misfit when growth on PBMO layer and positive misfit for the unit cell of PBMO growth on PMO. Modification of magnetic interaction was observed from the deduction of arrangement in magnetic spins ordering altered by deformation of crystal structure as well as the magnetic pinning effect among PMO and PBMO. The conducting route of PMO/PBMO or PBMO/PMO was follow PBMO layer which is lower in resistance. The highest %MR obtained from bi-layer films are lower compared to single layer PBMO (-50.0% at 80Kin 10kG magnetic field). The stacking sequence of PMO/PBMO promises higher %MR than PBMO/PMO.

Keywords: colossal magnetoresistance; magnetism; bi-layer thin film; structure and microstructure

INTRODUCTION

The revolution of Colossal Magnetoresistance (CMR) in perovskite manganite from single crystal to polycrystalline and even thin film nowadays not only studied in fundamental science but also for magnetic sensing application. Reduce costs and/or improve materials usage efficiency were the ultimate goals and this reviewed the importance of thin film technologies. However, transformation from bulk to thin film will modify its structure, microstructure, electrical transport and magnetic properties of the system. Such phenomenon becomes crucial in bi-layer and superlattices films by the accumulation of the lattice strain due to the epitaxial growth of the film which plays an important role in formation of the spin-ordered state and the value of CMR effect [1,2,3,4]. On the other hand, increasing lattice mismatch between substrate and film demonstrates physical changes via strain approach in describing the magnetic properties of manganite films [5,6,7]. In spite of the fact that the influence of single crystalline substrates on the magnetic and electronic properties of the manganite films which have

been quite well investigated. The development of hybrid devices such as oxide lattices are relatively few studies on ferromagnetic/paramagnetic [8,9], ferromagnetic/ferroelectric [10] and ferromagnetic/antiferromagentic [11]. Hence, more theoretical as well as experimental work is needed to understand such phenomena. In this work, investigation of structure, microstructure, magnetic and transport properties of single and bi-layer thin film in polycrystalline $PrMnO_3$ and $Pr_{0.67}Ba_{0.33}MnO_3$ manganite will be carried out.

METHOD

Bulk $PrMnO_3$ and $Pr_{0.67}Ba_{0.33}MnO_3$ were prepared via solid state reaction with stoichiometric amount of La_2O_3, $BaCO_3$, and $MnCO_3$ powders. These high purity powders (99.9%) were wet milled in acetone and dried at 100°C for 4 hours. Calcination at 900°C for 12 hours was introduced after the dried powders were ground. Subsequently, these powders were reground and sieved with 38µm sieve size before press into pellets. The pelletized powders were sintered at 1300°C for 24 hours. Thin film samples were fabricated via Pulsed Laser Deposition (PLD) technique on single crystal MgO oriented (100) substrate with bulk $PrMnO_3$ and $Pr_{0.67}Ba_{0.33}MnO_3$ as a target. The deposition was carried out using Nd-YAG laser of wavelength 1064nm with energy of 1.5 J/pulse at a pulse repetition rate of 10 pps. Before deposition, the substrate which located parallel 4 cm from the target was stabilized at 400°C in the oxygen pressured of 7×10^{-2} mbar. During deposition, the power density of the focused laser beam on the rotating target was about 4.7×10^{5} W/cm^2 and the deposition time was half an hour. After deposition, the film was cooled down slowly and trapped in surrounding of 2 mbar oxygen before post anneal in air at 700°C for 4 hours. Single layer thin films consist of $PrMnO_3$ (PMO) and $Pr_{0.67}Ba_{0.33}MnO_3$ (PBMO) whereas bi-layer thin films from coupling of PMO and PBMO with PMO growth on PBMO layer to form PMO/PBMO and vice versa for PBMO/PMO were fabricated.

The phase and crystal structure analysis was carried out by X-ray diffraction (XRD, Phillips PW 3040/60 Xpert Pro) technique and the collected data were analyzed using Rietveld refinement technique with X'Pert HighsScore Plus program. Field Emission Scanning Electron Microscope (FE-SEM, Zeiss SUPRA^{TM} 55VP) was used to analysis the microstructure. Magnetic properties were measured with Vibrating Sample Magnetometer (VSM, Lakeshore 7400 series). The electrical transports were measured with four-point probe method by Hall Measurement System (Lake Shore 7604 Hall Measurement System) with current in plane (CIP) and current perpendicular to plane (CPP) in cryostat with temperature ranging from 80 K to 300 K in 0T to 1T magnetic field, respectively.

RESULTS AND DISCUSSIONS

XRD spectra of all samples are shown in Figure 1. Rietveld refinement analysis shows that all samples are single phase in orthorhombic crystal structure. The refined

crystallographic data, lattice parameters and other fitting parameters of all samples were computed and tabulated in Table 1. The unit cell of PMO deformed and exhibit negative misfit when growth on PBMO. In fact, smaller unit cells (*a* and *b* axis) of PMO were growth on bigger unit cell of PBMO, unavoidable misfit would occur and generate lattice strain which could alter the crystal structure [12]. Thus, the lattice parameter, volume and density of the unit cell as well as the Mn-O-Mn bond angle and Mn-O bond length change corresponding to the lattice strain. Smaller crystallite size was observed from greater lattice strained crystal system. On the other hand, the unit cell of PBMO experience positive misfit when growth on PMO. This shows the importance of stacking sequence as the lattice misfit is correlated to the bottom layer to be growth in bi-layer film. The overall views of the changes in crystal structure were shown in Figure 2.

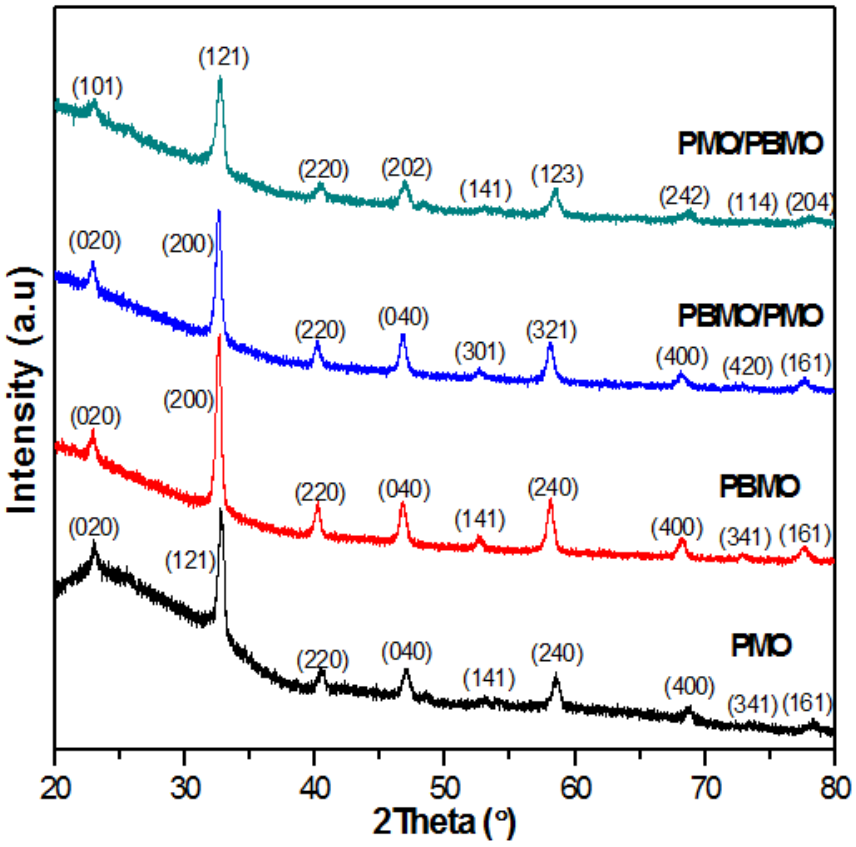

Figure 1: XRD spectra of PMO, PBMO, PMO/PBMO and PBMO/PMO thin films

Table 1: Refined crystallography data of PMO, PBMO, PBMO/PMO and PMO/PBMO.

Sample	**PMO**	**PBMO**	**PBMO/PMO**	**PMO/PBMO**
Crystal System	---------- Orthorhombic ----------			
Space Group	---------- *Pnma* ----------			
Lattice parameter				
***a* (Å)**	5.445 (2)	5.497 (2)	5.495 (1)	5.513 (2)
***b* (Å)**	7.703 (2)	7.758 (1)	7.752 (1)	7.709 (3)
***c* (Å)**	5.495 (4)	5.535 (2)	5.538 (2)	5.505 (2)
Volume (Å^3)	230.476	236.023	235.882	233.961
Density (g/cm^3)	7.026	6.806	6.832	7.003
Crys. size, D (nm)	18.9	22.2	21.1	13.4
Lattice strain (%)	0.715	0.620	0.651	0.986
Mn-O(1)-Mn (°)	155.3 (3)	150.8 (7)	167.5 (8)	148.1 (7)
Mn-O(2)-Mn (°)	142.8 (6)	163.0 (3)	133.2 (8)	159.5 (6)
Mn-O(1) (Å)	1.924 × 2	1.916 × 2	1.868 × 2 2.053 × 2	1.860×2 2.170×2
Mn-O(2) (Å)	2.333 × 2	2.114 × 2	2.115 × 2	1.956×2
R_{exp} (%)	2.148	2.834	2.903	2.783
R_{pr} (%)	2.430	2.558	2.543	2.838
R_{wpr} (%)	3.105	3.313	3.268	3.673
Goodness of fit	2.089	1.367	1.268	1.742

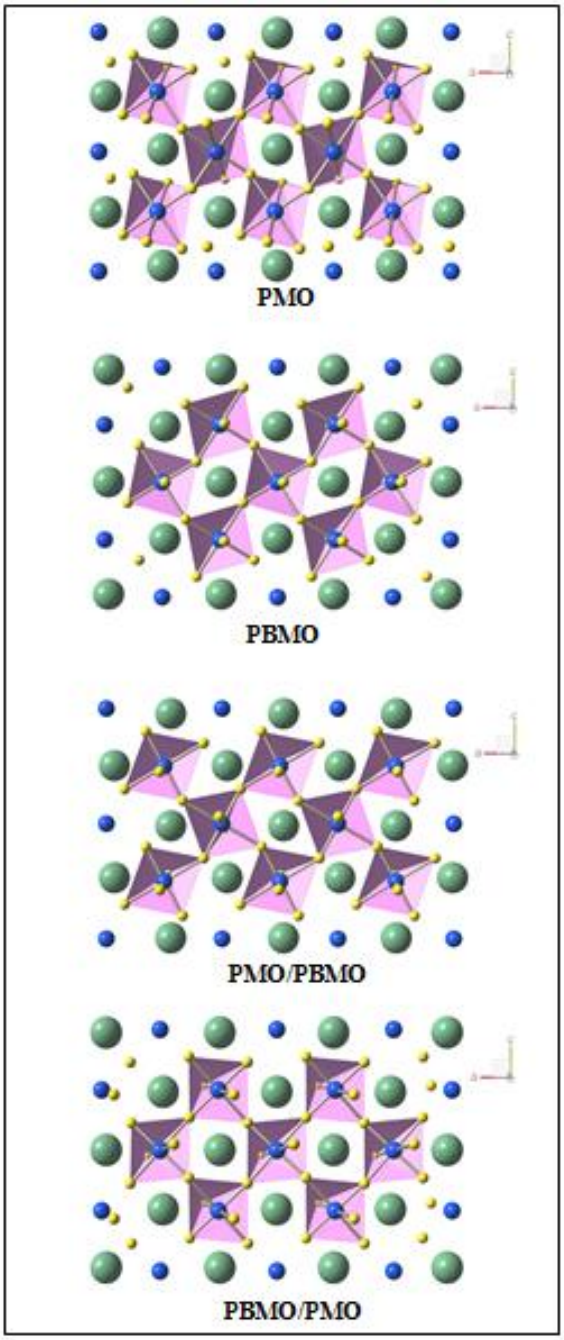

Figure 2: Schematic draw of crystal structure in PMO

Figure 3 shows the SEM micrographs of all thin film samples. Agglomeration of small particles (<100nm) to form a pile so-called grain was observed under magnification of 100,000X and due to strong diffusion the small particles necked. Minor island growth mode was expected since rounded piles of grain were observed. In fact, initially the

microstructure formation is layer-by-layer growth. Due to lattice misfit between film and substrate, strain was created and lead to island like growth. Hence, layer and island growth of microstructure formation is suggested in these samples. Overall, no significant change in microstructure can be seen.

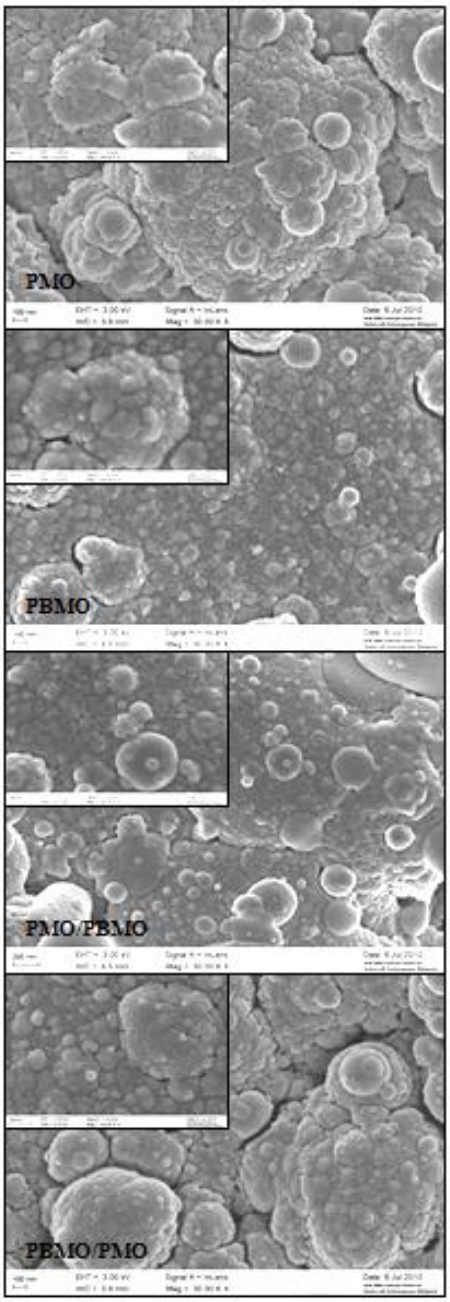

Figure 3: FE-SEM micrographs of PMO, PBMO, PMO/PBMO and PBMO/PMO thin films with magnification of 30,000X, the inset was 100,000X

The hysteresis loops of all samples as shown in Figure 4 show paramagnetic behavior. The highest magnetization values obtained in 10kG applied magnetic field for PBMO, PBMO/PMO, PMO/PBMO and PMO are 3.14, 1.10, 1.00 and 0.85 emu/g, respectively. The resultant magnetization of PBMO/PMO and PMO/PBMO are alike but relatively smaller as compared to single layer thin film of PBMO. Indeed, the spins tend to align according to the direction of the applied magnetic field but this effect seems weak in bi-layer films (lower magnetization). The magnetic spins in the coupled films might suffer from pinning effect among each layers and struggle in applied magnetic field [11]. At the same time, the paramagnetism contributed by PBMO layer might weakened when growth on PMO layer or PMO become more paramagnetism when growth on PBMO. In fact, their structure can be viewed as magnetically ordered small regions implanted in a matrix of disordered spins so-called 'cluster' glass state [13]. The change in Mn-O-Mn bond angle and Mn-O bond length due to lattice misfit induced by bottom layer could indirectly alter the magnetic spins order of top layer in bi-layer film. Hence, the depressed magnetization value in bi-layer films were related to the crystal structure deformation of the top layer and magnetic pinning effect among top and bottom layer in PBMO/PMO and PMO/PBMO system.

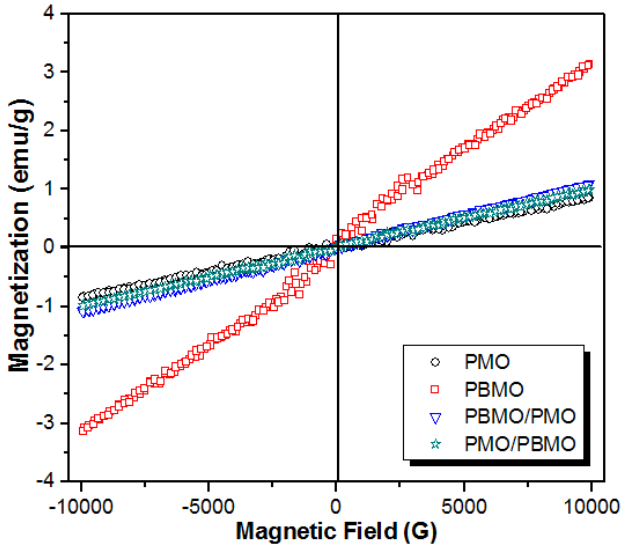

Figure 4: Hysteresis loops of PMO, PBMO, PBMO/PMO and PMO/PBMO taken at room temperature

The temperature variation of resistance from bi-layer films was measured with current in plane (CIP) and current perpendicular to plane (CPP) as shown in Figure 5 (a). All sample are insulator like with no significant transition temperature, T_P can be observed and might locate below 80K. The resistivity for PMO was not shown since it was antiferromagentic insulator manganites [14]. As compared, the resistance contributed by PBMO/PMO is higher than PMO/PBMO either measured with CIP or CPP.

The resistance measured with CIP or CPP configurations in PMO/PBMO bi-layer reveals similarity. Via CPP as shown in the schematic draw of Figure 5(a), the current is forced to flow from PMO to PBMO or vice versa in both layers. The bottom layer (PBMO) will serve as the main conduction route since its resistance is lower as compared to PMO. This phenomenon is further confirmed when the resistance obtained via CPP is comparable or near to the resistance of single layer PBMO. On the other hand, there is a possibility for the current to flow on top layer (PMO) or tunnel through top layer (PMO) follow by flowing in bottom layer (PBMO) with end up tunnel back to top layer (PMO) via CIP configuration (see schematic draw in Figure 5(a)). Since the measured resistance is quite close to the resistance of single layer PBMO via CIP, the conduction path should follows bottom layer (PBMO) rather than top layer (PMO) which is much higher in resistance.

However, in PBMO/PMO bi-layer the resistance obtained from CPP is higher than CIP. In CPP configuration, the current is force to flow from PMO to PBMO or vice versa in PBMO/PMO film. This higher resistance is mostly due to the current forced to pass through the PMO insulator layer. In CIP configuration, the resistance obtained was lower as compared to CPP configuration. The current most probably flow on top layer of PBMO rather than bottom layer (PMO). Yet, the resistance is higher as compared to single layer PBMO. This is mainly due to the distortion of crystal structure in top layer (PBMO) due to lattice misfit induced by bottom layer (PMO) as shown in Figure 2. Therefore, the Mn-O-Mn bond angle and Mn-O bond length are tilted and disturbed the electron conduction mechanism. Hence, the resistance measured from PBMO on top of PMO layer is slightly larger than resistance measured from single layer PBMO. Such observations reveal the influence of stacking sequence in electrical transport properties and become crucial in the magnetic field.

The percentage of MR is calculated using $\%MR= (R_H-R_o/R_o) \times 100$, where R_o and R_H is the resistance at zero and applied external magnetic field respectively. The %MR of all sample shows typical CMR behavior where %MR increase with further decrease of temperature in applied magnetic field (10kG) as shown in Figure 5 (b). The %MR shown by PMO/PBMO either measured with CIP or CPP configuration is similar to %MR of single layer PBMO. This observation further verifies that bottom layer (PBMO) in PMO/PBMO is the main current conduction path. The highest %MR was shown by PBMO (-50.0%) followed by PMO/PBMO (-47.4%) with CIP and PMO/PBMO with CPP (-47.8%) at 80K, respectively. Such small changes in %MR between single layer PBMO and bi-layer PMO/PBMO might be due to the magnetic pinning effect between PMO and PBMO film. The magnetic spins in bi-layer films are difficult or unable to align along the applied magnetic field direction.

On the other hand, comparison can be made where the %MR obtained from PMO/PBMO and PBMO/PMO are different in CIP configuration. As mentioned previously, deformation of crystal structure occurred in top layer (PBMO) of PBMO/PMO and altered the crystal structure. Such changes weakened the

magnetotransport properties governed by the double exchange mechanism and hence %MR of PBMO/PMO is relatively lower as compared to single layer PBMO. The low and scattered %MR was observed from PBMO/PMO in CPP configuration. As discussed previously, the main conduction path in PBMO/PMO-CPP is through PMO rather than PBMO. PMO is antiferromagentic insulator which has very small or no MR effect.

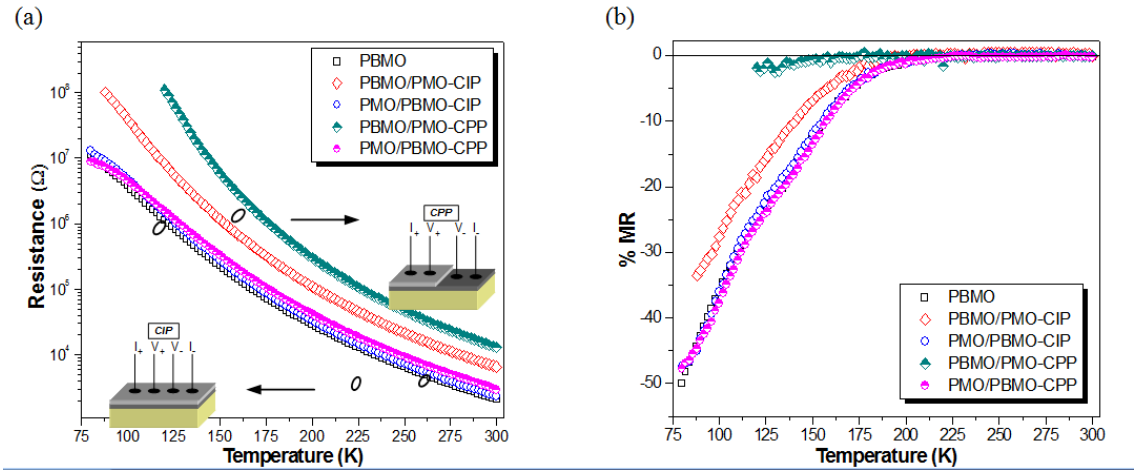

Figure 5: (a) Temperature variation of resistance in zero magnetic field and (b) %MR as a function of temperature in 10kG of applied external magnetic field. The measured current was in current in plane (CIP) and current perpendicular to plane (CPP).

CONCLUSION

The crystal structure, magnetic, electrical transport properties and magnetoresistive behavior of bi-layer thin film is stacking sequence dependent. Modification of crystal structure of top layer in bi-layer film could be done via lattice misfit generated from the characteristic of bottom layer to be grown. The induced crystal structure by lattice misfit not only could alter the magnetic spin ordering but also the electrical and magnetotransport properties of the system. The resistance measured from PBMO/PMO is slightly larger than resistance measured from single layer PBMO and/or PMO/PBMO.

ACKNOWLEDGEMENTS

The Ministry of Higher Education Malaysia (MOHE) is gratefully acknowledged for the grant under Research University Grant Scheme (RUGS) vote 91849: Low-Field Magnetoresistance effect in polycrystalline $Ln_{1-x}A_xMnO_3$ ceramic thin films and Ministry of Science, Technology and Innovation Malaysia (MOSTI) for National Science Fellowship (NSF) scholarship.

REFERENCES

[1]. H. S. Wang, E. Wertz, Y. F. Hu, L. Qi and D. G. Schlom. *Journal of Applied Physics* **87**(10), (2000) 7409-7414.
[2]. V. G. Prokhorov, G. G. Kaminsky, J. M. Kim, T. W. Eom, J. S. Park, Y. P. Lee, V. L. Svetchnikov, G. G. Levtchenko, Yu. M. Nikolaenko, and V. A. Khokhlov. *Low Temp. Phys.* **37**, (2011) 305.
[3]. V. G. Prokhorov, G. G. Kaminsky1, V. A. Komashko, Y. P. Lee, and J. S. Park. *Low Temp. Phys*. **29**, (2003) 663.
[4]. Y. P. Lee, S. Y. Park, V. G. Prokhorov, V. A. Komashko, and V. L. Svetchnikov. *Appl. Phys. Lett*. **84**, (2004) 777.
[5]. T. K. Nath, R. A. Rao, D. Lavric, C. B. Eom, L. Wu, and F. Tsui. *Appl. Phys. Lett*. **74**, (1999) 1615.
[6]. M. Bibes, L. Balcells, S. Valencia, and J. Fontcuberta, M. Wojcik, E. Jedryka, and S. Nadolski. *Phys. Rev. Lett*. **87**, (2001) 067210.
[7]. G. Srinivasan, E. T. Rasmussen, B. J. Levin, and R. Hayes. *Phys. Rev. B* **65**, (2002) 134402.
[8]. M. Egilmez, M. Abdelhadi, Z. Salman, K. H. Chow and J. Jung. *Applied Physics Letters* **95**, (2009) 112505.
[9]. V. G. Prokhorov, G. G. Kaminsky, V. A. Komashko, Y. P. Lee and J. S. Park. *Low Temperature Physics* **29**, (2003) 663-665.
[10]. V. G. Prokhorov, V. A. Komashko, and G. G. Kaminsky, K. K. Yu, S. J. Jun, S. Y. Park, J. S. Park, and Y. P. Lee and V. L. Svetchnikov. *Low Temp. Phys*. **33** (1), (2007) 58.
[11]. D. Kim. *Solid State Communications* **137**, (2006) 545-548.
[12]. G. Van Tendeloo, O. I. Lebedev, M. Hervieu and B. Raveau. *Reports on Progress in Physics* **67**(8), (2004) 1315-1365.
[13]. O. Pena, Y. Ma, M. Guilloux-Viry and C. Moure. *Applied Surface Science* **254**(1) (2007) 339–342.
[14]. E. L. Nagaev. *Physics Reports* **346** (2001) 387-531.